Supplemental Material for Discovery of unconventional charge density wave at the surface of $\mathbf{K_{0.9}Mo_6O_{17}}$

Daixiang Mou,[1,2] Aashish Sapkota,[1,2] H.-H. Kung,[3] Viktor Krapivin,[3] Yun Wu,[1,2] A. Kreyssig,[1,2] Xingjiang Zhou,[4] A. I. Goldman,[1,2] G. Blumberg,[3,5] Rebecca Flint,[1,2] and Adam Kaminski[1,2]

[1]*Division of Materials Science and Engineering,*
Ames Laboratory, U.S. DOE, Ames, Iowa 50011, USA
[2]*Department of Physics and Astronomy,*
Iowa State University, Ames, Iowa 50011, USA
[3]*Department of Physics and Astronomy,*
Rutgers University, Piscataway, NJ 08854, USA.
[4]*National Laboratory for Superconductivity,*
Beijing National Laboratory for Condensed Matter Physics,
Institute of Physics, Chinese Academy of Sciences, Beijing 100190, China
[5]*National Institute of Chemical Physics and Biophysics, 12618 Tallinn, Estonia.*

(Dated: April 11, 2016)

I. SAMPLES

$K_{0.9}Mo_6O_{17}$ single crystals were grown by electrolytic reduction. K_2CO_3 and MoO_3 mixed power with molar ratio of 1:6 was melt at ∼580°C in an alumina crucible and an electric current of ∼40 mA was applied through the melt by platinum wire electrodes. Single crystals were obtained on the cathode after three hours. The typical size of the samples was $\sim 2 \times 2 \times 0.3\,\mathrm{mm}^3$ in ARPES measurements and $\sim 3 \times 4 \times 1\,\mathrm{mm}^3$ in the x-ray diffraction measurements.

II. ARPES

Samples were cleaved *in situ* at a base pressure lower than 8×10^{-11} Torr. They were cooled using a closed cycle He-refrigerator and the sample temperature was measured using a silicon-diode sensor mounted on the sample holder. The energy corresponding to the chemical potential was determined from the Fermi edge of a polycrystalline Au reference in electrical contact with the sample. Samples were cleaved at three temperatures (40 K, 130 K and 260 K) to check the stability of the surface structure. The real part of self energy was obtained by subtracting fitted parabolic dispersion from actual measured dispersion using lorentzian fits to MDCs. The imaginary part of the self energy was obtained by fitting MDC data with lorentzians, and dividing their half-widths by the velocity determined by parabolic fit to the dispersion.

III. XRAY

Two-dimensional diffraction patterns of the $(H\ K\ 0)$ reciprocal plane were measured for overview using a MAR345 detector after rocking the sample through two independent angles up to ±1.8° about axes perpendicular to the incident beam. The sample was mounted on the cold finger of an APD He closed–cycle refrigerator. A detailed study of the temperature dependence of the $(\frac{9}{2}\ 0\ 0)$ CDW Bragg peak was performed using the high-resolution Pixirad detector by rocking the sample through one angle by ±5°. The integrated intensity of the CDW peaks was obtained from fitting two-dimensional Gaussian peaks.

IV. RAMAN

The $K_{0.9}Mo_6O_{17}$ compound crystallizes in a trigonal structure (space group $P\overline{3}$, No. 147) belonging to the C_{3i} point group [47]. The structure allows a total of 72 phonon modes at the Brillouin zone center (Γ point), categorized by the irreducible representations of the C_{3i} group: A_u+E_u acoustic modes, $13A_u+13E_u$ infrared active modes, and $10A_g+10E_g$ Raman active modes. Polarized Raman scattering measurements from the *ab* surface of the single crystal were performed in quasi-backscattering geometry using the 530.9 nm excitation line of a Kr^+ ion laser with less than 15 mW of incident power focused to a $50 \times 100\,\mu m^2$ spot. The sample was cleaved in air immediately before loading into a continuous flow helium cryostat. The temperatures quoted have been corrected for the laser heating. We used a custom triple-grating spectrometer and liquid nitrogen cooled CCD detector for collection and analysis of the scattered light. The data were corrected for the spectral response of the spectrometer and the CCD. The Raman response function, $\chi''(\omega, T)$, measures the electronic and phononic excitations with E_g symmetry (C_{3i} group) when the scattered photon are analyzed in the polarization perpendicular to the incident excitation polarization, which is aligned with the crystallographic *a*-axis, whereas excitations with both $A_g + E_g$ symmetry (C_{3i} group) are probed when the scattered photon are analyzed in the polarization parallel to the incident excitation polarization.

Figure S2 shows the Raman response function in the E_g (blue) and $A_g + E_g$ (red) symmetries. The 10 Raman active E_g and A_g optical phonons are labeled by symmetries (top axis) and energies in blue and red, respectively. The phonon frequencies have increased slightly, whereas the widths have narrowed with decreasing temperature, both owing to the anharmonic decay effects [55]. No other changes in the phonon energies are observed across both bulk and surface transitions in these data for purple bronze, in contrast to materials where new phonon modes appear in the CDW phase [56, 57]. Fig. S3 shows the temperature dependence of the integrated phonon intensity. Most phonons show only weak temperature dependence. In contrast, $E_g^{(6)}$, $E_g^{(9)}$ and $E_g^{(10)}$ phonons display almost two fold increase of integrated intensity intensity on cooling, where the temperature dependence show some evidence of coupling to the surface CDW order parameter below 250 K.

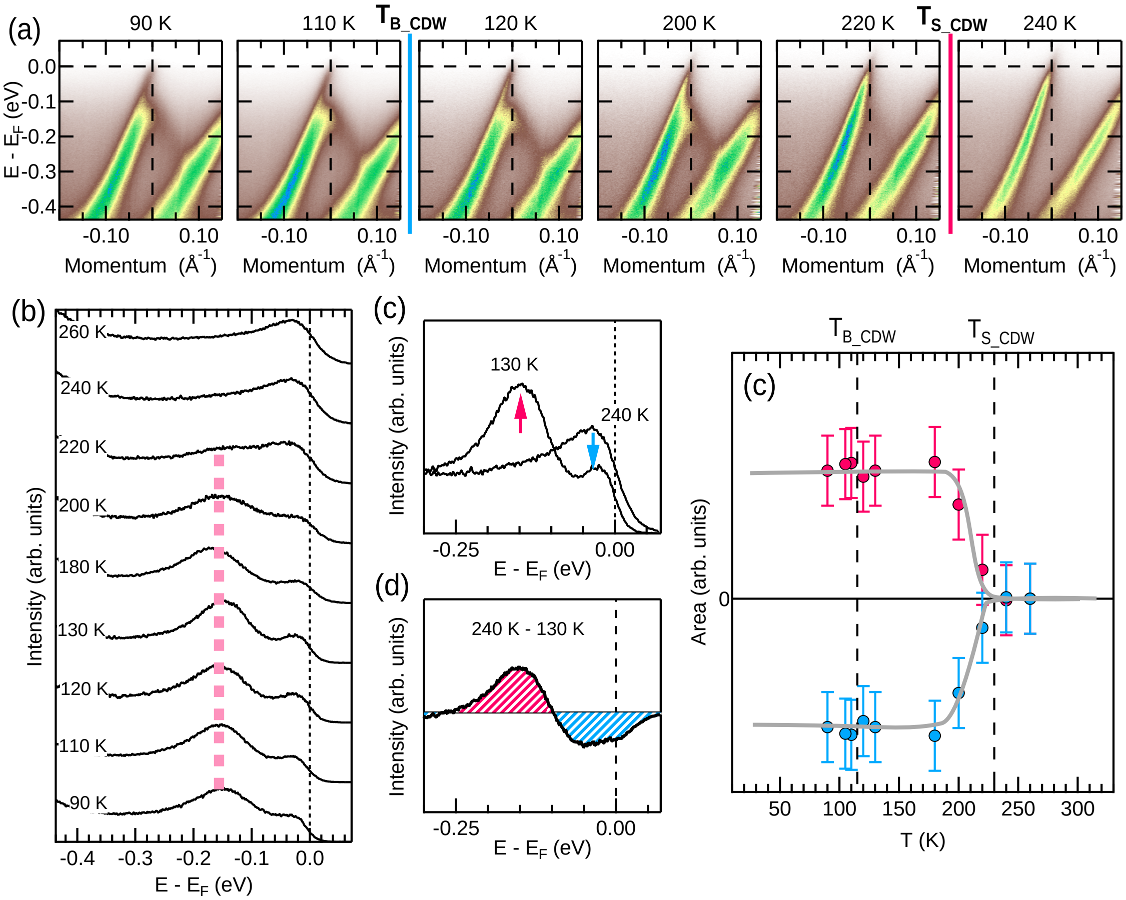

FIG. S1. Temperature dependent intensity of bulk and surface branches. (a), Temperature dependence of the electronic structure. Cut position is the same as shown in Fig. 1. T_{B_CDW}(∼115 K) marks the bulk CDW transition temperature and T_{S_CDW}(∼230 K) marks the temperature of the onset of the back bending band. (b), Extracted k_F EDCs at different temperatures. Data are offset vertically for clarity. The peak structure around 150 meV due to the band back bending disappears at T_{S_CDW}. (c), k_F EDC lines at 240 K and 130 K. Data are normalized to the total intensity between -0.35 eV and 0.07 eV. Two arrows indicate the redistribution of electron density from 240 K to 130 K. (d), Electron density difference between 240 K and 130 K of EDCs at k_F. (e), Electron density redistribution across T_{S-CDW}. Data are obtained by adding the positive area around -150 meV and the negative area around E_F as illustrated in d. The sudden redistribution of electron density from E_F to high binding energy is consistent with the opening of a ∼150 meV gap on the surface band below T_{S_CDW}.

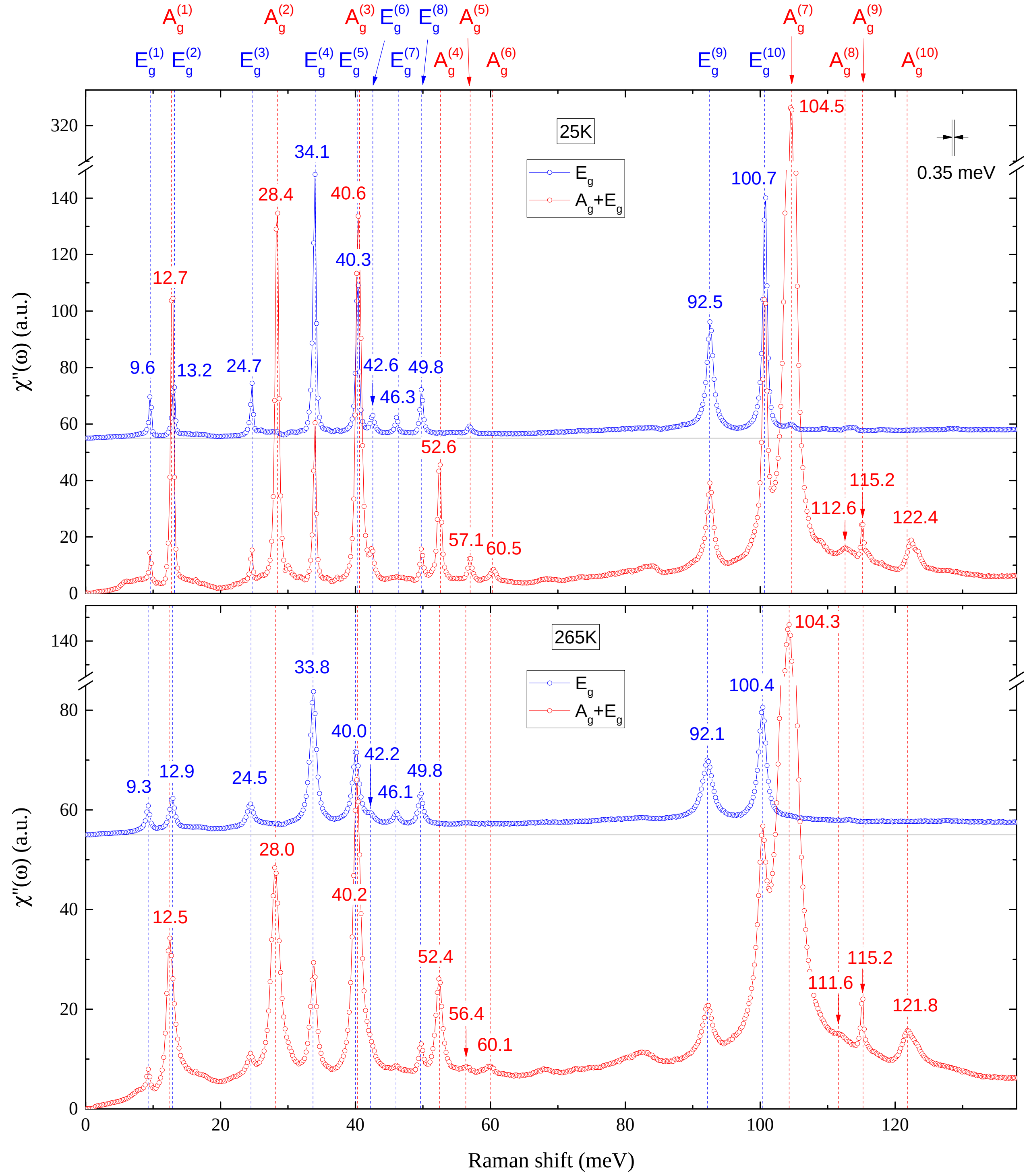

FIG. S2. The Raman response, $\chi''(\omega, T)$, probing the E_g (blue) and $A_g + E_g$ (red) symmetries (D_{3i} group) are plot against Raman shift for 265 K and 25 K. The data are shifted for clarity. The energies associated with the bulk phonons with E_g and A_g symmetries are labeled next to the phonon peaks in blue and red, respectively.

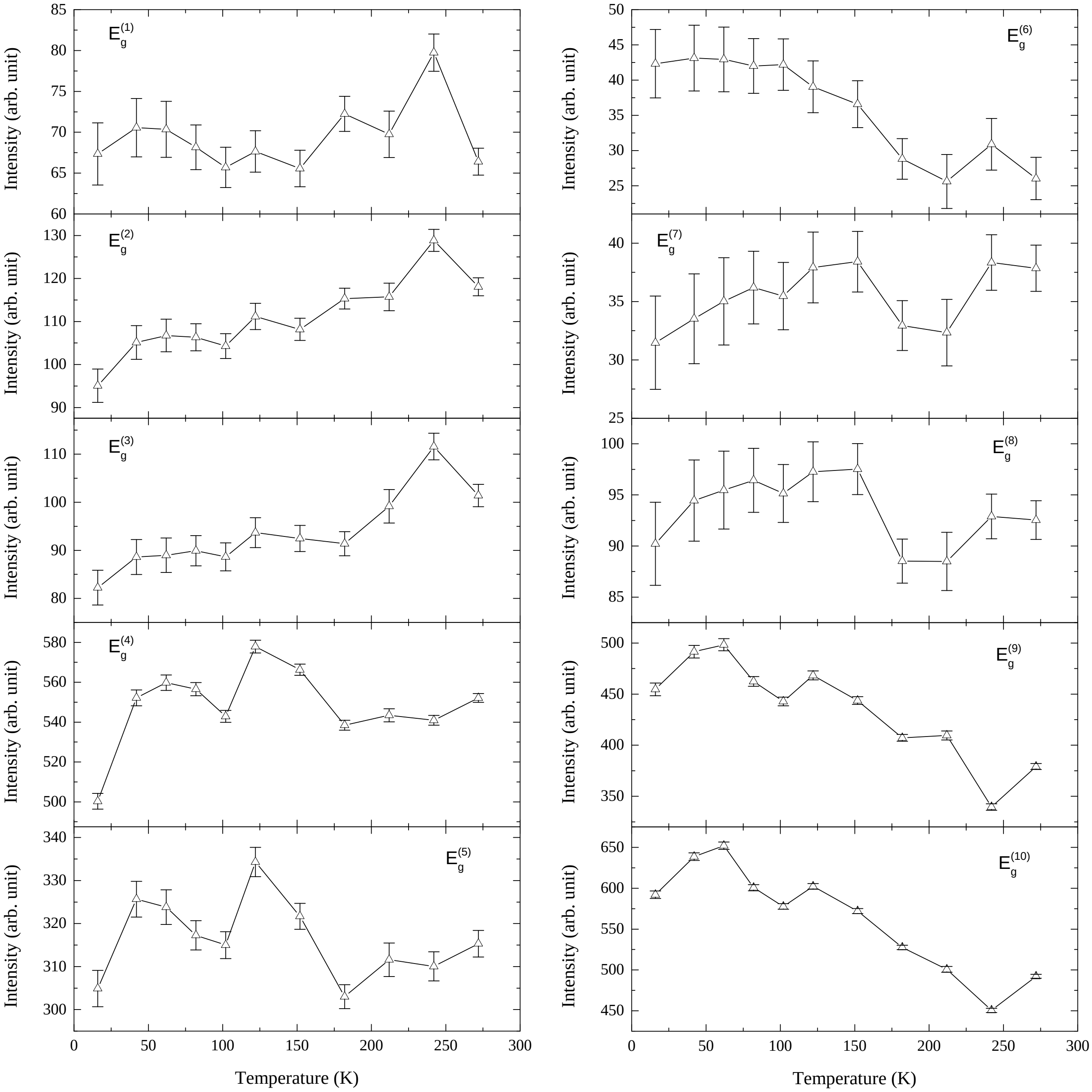

FIG. S3. The temperature dependence of integrated phonon intensity for the 10 Raman active E_g phonons. The error bars show standard error to Voigt function fits.